Cell Biol Toxicol (2025) 41:56
https://doi.org/10.1007/s10565-025-10007-9

RESEARCH

Andrographolide ameliorates sepsis-induced acute liver injury by attenuating endoplasmic reticulum stress through the FKBP1A-mediated NOTCH1/AK2 pathway

Jiaqi He · Zepeng Huang · Rui Zou

Received: 18 November 2024 / Accepted: 20 February 2025

Abstract Andrographolide (AP) has been shown to possess anti-inflammatory activities. In this study, the impact of AP in sepsis-induced acute liver injury (ALI) and the molecules involved were dissected. FKBP1A was predicted to be the sole target protein of AP that was also differentially expressed in the GSE166868 dataset. AP induced the protein expression of FKBP1A and suppressed that of NOTCH1 in a dose-dependent manner. AP ameliorated ALI in mice induced by D-galactosamine and LPS and inhibited LPS-induced liver parenchymal cell injury in vitro. By contrast, the protective effect of AP was significantly lost after the knockdown of FKBP1A. As a positive control, the therapeutic effect of dexamethasone on ALI may be related to NOTCH1, which was not related to FKBP1A. NOTCH1 promoted AK2 transcription in liver parenchymal cells, and FKBP1A inhibited endoplasmic reticulum (ER) stress by impairing NOTCH1/AK2 signaling. Restoration of NOTCH1 significantly reversed the hepatoprotective effect of AP in ALI mice and LPS-induced liver parenchymal cell injury by activating the ER stress pathway. Therefore, AP-promoted FKBP1A expression inhibits ALI progression by blocking the NOTCH1/AK2-mediated ER pathway.

Keywords Andrographolide · Acute liver injury · FKBP1A · NOTCH1 · Endoplasmic reticulum stress

Introduction

As demonstrated in the data published in 2020, the global incidence of sepsis-related deaths was 48.9 million cases, constituting 19.7% of all global deaths (Cecconi et al. 2018; Rudd et al. 2020). Sepsis-induced acute liver injury (ALI) is recognized as an independent predictor of mortality in the intensive care unit (ICU) (Sun et al. 2020). The precise incidence of sepsis-related liver dysfunction remains challenging to ascertain due to the absence of a definitive and consensus definition, as well as the heterogeneity of the observation periods, and liver failure was observed in 12% of cases in a cohort of 1,342 episodes of sepsis syndrome within 28 days following the onset of the disease (Nesseler et al. 2012). Sepsis

Supplementary Information The online version contains supplementary material available at https://doi.org/10.1007/s10565-025-10007-9.

J. He
Department of General Surgery, Huadong Hospital Affiliated to Fudan University, Shanghai 200040, P.R. China

Z. Huang · R. Zou (✉)
Department of Hepatobiliary Surgery, Hainan Cancer Hospital, Haikou 570000, Hainan, P.R. China
e-mail: zourui@hainmc.edu.cn

R. Zou
Hainan Clinical Research Center for Liver Disease and Liver Critical Illness, Haikou 570000, Hainan, P.R. China

Published online: 07 March 2025

is a particularly problematic condition in patients with liver cirrhosis due to the increased bacterial translocation from the gut and impaired microbial defense that these patients experience and can induce acute on chronic liver failure, which was related to high short-term mortality (Strnad et al. 2017). The association between septic liver dysfunction and mortality has been a subject of considerable research interest, while the extant literature has yet to address the question of whether such dysfunction impacts long-term mortality in cases of septic shock (Nesseler et al. 2016). The dysfunction of the liver is indicative of a critical event in multiple organ dysfunction syndrome, which is associated with the immunological, regulatory, and metabolic functions of liver parenchymal cells (Perez Ruiz de Garibay et al. 2022). Therefore, an in-depth exploration of the mechanisms of sepsis-induced ALI and the role of liver parenchymal cells in it have great significance for discovering new targets for the treatment of patients in the ICU.

Andrographolide (AP) is a type of natural compound identified as the primary bioactive constituent of the plant *Andrographis paniculata* with documented applications in the management of various health conditions associated with inflammation (Dai et al. 2019; Low et al. 2024). For instance, AP has been suggested to alleviate dextran sulfate sodium-induced ulcerative colitis (Shu et al. 2024), porcine pancreas elastase/lipopolysaccharide (LPS)-induced chronic obstructive pulmonary disease (Yu et al. 2024), atorvastatin-mediated zebrafish brain injury (Zhou et al. 2024), and LPS-induced acute lung injury (Li et al. 2024). It is imperative to acknowledge the pivotal function of AP in the context of liver disease phenotypes, primarily through its anti-inflammatory and antioxidant properties (Qin et al. 2023). In this study, we sought to further expound the molecular mechanism involved in this hepatoprotective effect. Based on an online prediction server and a GEO database (GSE166868), we obtained the only possible target protein of AP in ALI: FK506-binding protein 1a (FKBP1A, also known as FKBP12). It is an immunophilin protein that binds the immunosuppressant drugs FK506 and rapamycin, which can be used for treating organ transplant rejection and other diseases (Gant et al. 2014). Interestingly, FKBP1A has been identified as a novel negative modulator of activated NOTCH1 in ventricular hypertrabeculation (Chen et al. 2013). NOTCH1 expression in liver macrophages exhibited a strong correlation with LPS/D-galactosamine-induced ALI, and the induction of hepatocellular apoptosis was significantly mitigated in myeloid-specific NOTCH1 knockout mice. (Yang et al. 2023). Furthermore, the promotion of NOTCH1 levels was found at 3 h following the LPS challenge in RAW 264.7 cells, and disruption of the Notch signaling by DAPT has been shown to attenuate the LPS-induced inflammatory responses, with a concomitant improvement in experimental sepsis survival (Tsao et al. 2011). However, the impact of FKBP1A-mediated NOTCH1 on liver parenchymal cells remains obscure. Lastly, adenylate kinase 2 (AK2), a gene closely related to unfolded protein response induction and the ensuing endoplasmic reticulum (ER) stress (Burkart et al. 2011), was identified as the target of the transcription factor NOTCH1 in ALI. AP has also been recently reported to attenuate cardiac hypertrophy by suppressing ER stress (Tian et al. 2023). This study was conducted to verify the hypothesis that AP can attenuate ER stress, thereby alleviating ALI in mice by restoring NOTCH1 and suppressing NOTCH1-mediated AK2.

Materials and methods

Cell culture and LPS treatment

Mouse primary liver parenchymal cells (CTCC-D017-MIC, Meisen Cell, Jinhua, Zhejiang, China) were cultured using the liver parenchymal cell culture system (CTCC-008-PriMed, Meisen Cell) at 37 °C with 5% CO_2.

Short hairpin RNA (shRNA) sequences of FKBP1A and AK2 (sh-FKBP1A #1 ~ #3; sh-AK2 #1 ~ #3), the overexpression plasmids of NOTCH1 (Vector-NOTCH1), and the respective controls (sh-Scramble, Vector-NC) used for cell transfection were purchased from VectorBuilder (Guangzhou, Guangdong, China). The above plasmids (shRNAs) were transfected into liver parenchymal cells using Lipofectamin2000 (11,668,500, Thermo Fisher), and the following assays were performed 48 h later.

To analyze the dose-dependent toxicity of AP on liver parenchymal cells, they were treated with graded concentrations of AP (0, 10, 20, 40, 60, 80 μM; catalog number: V0768; InvivoChem, Guangzhou, Guangdong, China) for 6 h. Primary liver

Table 1 Histopathological Scoring system of liver tissues

Score	Description
0	No hepatocellular injury
1	Very few cells with hyperemia, vacuolization, or single cell necrosis
2	Few cells with hyperemia, vacuolization, or necrotic in < 30% of the area
3	Majority of the cells with hyperemia, vacuolization, or necrotic in < 60% of the area
4	Severe hemorrhage and necrotic in > 60% of the area

parenchymal cells were incubated with LPS (500 ng/mL) for 6 h in the presence or absence of AP to mimic ALI, and normal saline (NS)-treated primary liver parenchymal cells were used as a control (Liu et al. 2020).

Animals and treatments

The study protocols were approved by the Institutional Animal Care and Use Committee of the Huadong Hospital Affiliated to Fudan University (approval number: 2021K010, experimental animal's use license: SYXK (Shanghai) 2020–0032). Male C57BL/6 mice (8-weeks, 22–25 g, catalog number: VSM10001) were purchased from Viewsolid (Beijing, China). Referring to a previous report (Zhang et al. 2020), sepsis-induced ALI was developed in mice by injection of 200 mg/kg D-galactosamine (G0500, Sigma-Aldrich Chemical Company, St Louis, MO, USA) and 3 mg/kg LPS (L2630, Sigma-Aldrich), *i.p.* NS-treated mice were used as controls. The animals were observed for survival ($n = 8$ for each group), and the surviving mice were euthanized by sodium pentobarbital at 150 mg/kg *(i.p.)* 36 h after ALI modeling. Serum and liver tissues were collected. Five mice were randomly selected from each group.

Mice requiring AP treatment were gavaged with graded concentrations of AP (20, 50, 100 mg/kg) once daily for 8 consecutive days (Ye et al. 2011). Immediately after the last gavage, the mice were injected with D-galactosamine and LPS to develop the ALI mouse model. The ER stress inhibitor tauroursodeoxycholate (TUDCA, HY-19696, MedChemExpress, Monmouth Junction, NJ, USA) was added to drinking water at a dose of 0.5 g/kg/day (same time as AP treatment) (Qin et al. 2017). For the positive control of AP treatment, 1 mg/kg dexamethasone (DEX, HY-14648, MedChemExpress) was injected subcutaneously into mice (Santos et al. 2001) 1 h before ALI modeling.

Gene expression manipulation was achieved by a single injection of 100 µL of the corresponding lentivirus into the tail vein of mice. The lentiviruses harboring sh-FKBP1A #1 (named LV-FKBP1A^{KD}), the overexpression lentivirus of NOTCH1 (named LV-NOTCH1^{OE}), and the respective control viruses (LV-NC^{KD}, LV-NC^{OE}) were obtained from VectorBuilder. Lentiviral titer was 10^9 TU/mL, and ALI modeling was performed 2 weeks after lentiviral injection.

Histology and immunohistochemistry (IHC)

Mouse livers were fixed with 4% paraformaldehyde (PFA, P0099, Beyotime, Shanghai, China), paraffin-embedded, and sectioned at 4 µm. After being deparaffinized and hydrated, staining was performed by hematoxylin–eosin (HE) staining solution in the HE Staining Kit (C0105S, Beyotime) for 5 min and by eosin staining solution for 1 min. Histopathological results were assessed microscopically on a scale of 0 to 4 (Zhang et al. 2020a). The specific histopathological score criteria are described in Table 1.

Liver sections were sealed with 10% goat serum (SBJ-SE-GO012, SenBeiJia, Nanjing, Jiangsu, China) for 1 h and treated with 3% H_2O_2 (H792073, Macklin, Shanghai, China). The sections were incubated with primary antibodies (Table 2) and with the secondary antibody at room temperature (RM) for 1 h. Positive staining was visualized using the DAB HRP color development Kit (P0203, Beyotime), followed by hematoxylin counter-staining. The sections were viewed under a light microscope (Olympus Optical Co., Ltd., Tokyo, Japan), and positive staining was quantified by ImageJ software.

For dual-labeling immunohistochemistry, rabbit anti-FKBP1A or NOTCH1 was used, followed by re-probing with a secondary antibody for 1 h at RM in darkness. Live parenchymal cells were labeled by Alexa Fluor 488-coupled mouse anti-Cytokeratin 18 (CK-18) at RM for 1 h in darkness, and the nuclei

Table 2 List of antibodies used in this study

Antibodies	Company	Catalog number	Dilution	Application
FKBP1A	ProteinTech Group	10,273–1-AP	1:200, 1:1000	IHC, WB
NOTCH1 (Cleaved Val1744)	Thermo Fisher Scientific	PA5-99,448	1:200, 1:2000	IHC, WB
CHOP	ProteinTech Group	15,204–1-AP	1:500, 1:1000	IHC, WB
GRP78	ProteinTech Group	11,587–1-AP	1:500, 1:1000	IHC, WB
AK2	ProteinTech Group	11,014–1-AP	1:500, 1:2000	IHC, WB
HES1	Beyotime	AF2167	1:200	IHC
Goat anti-rabbit IgG H&L (HRP)	Abcam	ab6721	1:1000, 1:10000	IHC, WB
Alexa Fluor 647 labeled goat anti-rabbit IgG (H + L)	Beyotime	A0468	1:200	IHC
Alexa Fluor 488-coupled mouse anti-CK-18	Thermo Fisher Scientific	MA5-18,157	1:200	IHC
β-actin	ProteinTech Group	81,115–1-RR	1:5000	WB

of the cells were counter-stained by DAPI (C1006, Beyotime). After sealing, the sections were viewed under a fluorescence microscope.

Biochemical analysis

Cytokine concentrations in mouse serum samples or cell culture supernatant from liver parenchymal cells were examined using Mouse ALT ELISA Kit (CSB-E16539m), AST ELISA Kit (CSB-E12649m), TNF-α ELISA Kit (CSB-E04741m), and IFN-γ ELISA Kit (CSB-E04578m). All operations are carried out according to the manufacturer's (Cusabio Biotech, Newark, DE, USA) protocols.

Western blot analyses

Protein extracts of liver parenchymal cells were prepared in RIPA lysis buffer (89,901, Thermo Fisher Scientific). After quantification, equal amounts of proteins (20 μg) were separated by 10%−12% SDS-PAGE and transferred to a PVDF membrane. After being sealed with 5% BSA, the membranes were probed with primary antibodies (Table 2) overnight at 4 °C and with the secondary antibody at RM for 1 h. Finally, target protein blots were visualized by enhanced chemiluminescence using the BeyoECL Plus kit (P0018M, Beyotime) and quantified by ImageJ.

CCK-8 assay

Liver parenchymal cells were plated into 96-well plates at 5000 cells/well and subjected to the indicated treatment (LPS or/and AP). Subsequently, 10 μL of CCK-8 solution (C0037, Beyotime) was added to the cells, and incubation was continued for 2 h at RM. The relative viability of the cells was analyzed by reading the OD at 450 nm and normalizing to the control.

TUNEL assay

One-Step TUNEL Apoptosis Assay Kit (YT135, Biolab, Beijing, China) was used. For liver parenchymal cells, the cells were treated with 4% PFA for 30 min, with PBS (C0221A, Beyotime) containing 0.3% Triton X-100 (QN0247, Biolab, Beijing, China) for 5 min at RM, and with the TUNEL assay solution for 1 h in darkness. After counter-staining the nuclei with DAPI and blocking with an anti-fluorescence quenching blocking solution, the cells were viewed under a fluorescence microscope (Carl Zeiss, Oberkochen, Germany). For mouse liver sections, 20 μg/mL of DNase-free proteinase K (ST535, Beyotime) was supplemented dropwise for a 30-min incubation at 37 °C. The remaining staining steps were the same as for cell staining.

RT-qPCR

Total RNA was isolated from liver parenchymal cells using TRIzol (15596018CN, Thermo Fisher) and

Table 3 List of primers used in this study

Gene	Forward primer (5'−3')	Reverse primer (5'−3')	Catalog number
NOTCH1	GCTGCCTCTTTGATGGCTTCGA	CACATTCGGCACTGTTACAGCC	MP209021
AK2	TGAAGGCGACAATGGATGCAGG	GCATTTCAGCCTGCCTCACAGT	MP200395
LASP1	AGCAGATGACCTCGTCCTATGG	CATCCTGGAAGGAGACCTCGTC	MP207512
β-actin	CATTGCTGACAGGATGCAGAAGG	TGCTGGAAGGTGGACAGTGAGG	MP200232

converted to cDNA using the HiScript II 1st Strand cDNA Synthesis Kit (R211-01, Vazyme, Nanjing, Jiangsu, China). The cDNA obtained from reverse transcription was subjected to a tenfold gradient dilution, followed by the qPCR reaction using AceQ qPCR SYBR Green Master Mix (Q121, Vazyme) on a Bio-Rad CFX96. At the end of the qPCR reaction, a calibration curve was made using the cDNA dilution log value as the X-axis and the corresponding Ct value as the Y-axis. According to the MIQE guidelines: minimum information for publication of quantitative real-time PCR experiments (Bustin et al. 2009), amplification efficiency determined from the slope of the log-linear portion of the calibration curve, with PCR efficiency $= 10^{-1/\text{slope}} - 1$. The PCR efficiency of all primers used was greater than 90%. The gene expression was calculated using the $2^{-\Delta\Delta\ Ct}$ method, and the primer sequences (OriGene Technologies, Beijing, China) are provided in Table 3.

ChIP assay

The Pierce Agarose ChIP Kit (26,156, Thermo Scientific) was used. Liver parenchymal cells were cross-linked with 1% formaldehyde, and chromatin was sheared by proteinase K and micrococcal nuclease. Immunoprecipitation was then performed with anti-NOTCH1 (1:200, MA5-35,256, Invitrogen Inc., Carlsbad, CA, USA) or normal rabbit IgG (1:200, Thermo Scientific), and immunoprecipitated DNA was collected and purified. The extent of AK2 promoter enrichment was analyzed by qPCR.

Luciferase assays

An AK2 promoter luciferase reporter was generated by inserting the promoter fragment of AK2 into the pGL3-Basic vector (E1751, Promega Corporation, Madison, WI, USA). Liver parenchymal cells were plated into 96-well plates and cultured to 70% confluence. Overexpression DNA vectors and control vectors of NOTCH1 and AK2 promoter reporter were transfected into cells using Lipofectamin2000 for 48 h. The Dual-Luciferases Reporter Assay System (E1910, Promega) was used for evaluation.

Quantification and statistical analyses

The sample size for the animal experiments ($n = 8$ or 5/group) was based on a published report (Wu et al. 2022). It was confirmed that the power of the test(1-β) was greater than 0.8 at $\alpha = 0.05$ for all the selected sample sizes using post hoc analysis in Gpower software (v3.1.9.7). All data are presented as mean ± SEM. The difference between the two groups was tested by unpaired t-tests, and the difference between multiple groups was assessed by one-way ANOVA, followed by Tukey's or Dunnett's post hoc test using GraphPad Prism 8.0.2 (GraphPad, San Diego, CA, USA). Differences between multiple groups were statistically significant when $p < 0.05$.

Results

AP promotes protein expression of FKBP1A in liver tissues of mice concentration-dependently

Based on the chemical structure of AP (PubChem CID: 5,318,517) (Fig S1A), the target proteins of AP were predicted in SuperPred (https://prediction.charite.de/index.php) (Fig S1B). To screen for therapeutic targets in ALI, transcriptome differences in liver tissues of mice with LPS-induced ALI were analyzed in the GSE166868 dataset (https://www.ncbi.nlm.nih.gov/geo/query/acc.cgi?acc=GSE166868), and genes that were significantly differentially expressed were screened at $p < 0.05$ (Fig S1C). The intersection of the two datasets revealed only one intersecting target: FKBP1A (Fig S1D). FKBP1A has been identified as

a novel negative modulator of activated NOTCH1 (Chen et al. 2013). Therefore, we hypothesized that AP might ameliorate ALI by blocking NOTCH1 signaling through enhanced protein expression of FKBP1A.

Mice were pretreated with a graded dose of AP (DEX was used for the positive control), and an ALI mouse model was subsequently developed by intraperitoneal injection of D-galactosamine and LPS. ALI modeling resulted in a certain number (2/8) of mice dying within 36 h. AP pretreatment prolonged the survival of ALI mice to a certain extent, in which none of the mice pretreated with 100 mg/kg AP or DEX died within 36 h after ALI modeling. Still, the difference was not significant (Fig S1E). On the one hand, this was because the number of mice in each group ($n=8$) may be too small, and too many confounding factors caused by the multiple-group analysis. On the other hand, even in the ALI group with the lowest survival rate, the 36-h survival rate was still 75% (6/8), resulting in insufficient variability in the difference in survival rate between it and the groups with no mouse deaths. The increase of ALT and AST levels in serum samples of mice confirmed the occurrence of liver injury in ALI-modeled mice, and high doses of AP and DEX pretreatment were effective in exerting hepatoprotective effects (Fig S1F).

It was observed using HE staining that AP and DEX treatments significantly ameliorated D-galactosamine and LPS-induced pathologic changes in liver tissue structure and lowered histopathological score (Fig. 1A). FKBP1A expression was downregulated and the cleaved-NOTCH1 (notch intracellular domain) expression was enhanced in the liver tissues of ALI mice. AP treatment promoted intrahepatic FKBP1A (Fig. 1B) expression and blocked active protein expression of NOTCH1 (Fig. 1C) expression in a concentration-dependent manner. The positive control DEX also inhibited NOTCH1 expression, but this was not dependent on FKBP1A expression. IHC for HES1 also confirmed activation of NOTCH signaling in ALI with elevated HES1 expression, which was suppressed by AP treatment (Fig. 1D).

Using the specific marker CK-18 for labeling of liver parenchymal cells (Du et al. 2013), we observed attenuated expression of CK-18 in ALI mice, representing the onset of liver parenchymal cell injury, as well as a significant decrease in FKBP1A expression (Fig. 1E) and elevated expression of cleaved-NOTCH1 (Fig. 1F) in liver parenchymal cells. AP promoted FKBP1A expression in liver parenchymal cells in a concentration-dependent manner, blocked NOTCH1 activation, and ameliorated liver parenchymal cell loss (Fig. 1E, F). The positive control DEX also inhibited NOTCH1 activation and ALI-induced hepatic parenchymal cell injury but did not affect FKBP1A expression. The dose of 100 mg/kg was used in subsequent animal experiments, and liver parenchymal cells were used for in vitro assays.

AP-induced FKBP1A ameliorates liver parenchymal cell injury by blocking NOTCH1 signaling

Mouse liver parenchymal cells were treated with AP at different doses, and AP was not significantly toxic to these cells until 60 μM concentration (Fig. S2).

Western blot assay detected a significant attenuation of FKBP1A protein expression in LPS-treated liver parenchymal cells, and abnormal activation of NOTCH1 was observed. In contrast, the expression of FKBP1A was rescued by AP treatment and the expression of active NOTCH1 was inhibited (Fig. 2A). Cells were pre-transfected with shRNA sequences of FKBP1A and treated with LPS and AP. ShRNAs targeting FKBP1A downregulated FKBP1A expression and restored NOTCH1 expression in the cells (Fig. 2B). The sh-FKBP1A #1 with the best knockdown efficiency was used in the subsequent assays.

LPS treatment decreased the viability of liver parenchymal cells. AP attenuated LPS-induced cellular injury, but the protective effect of AP was significantly lost in cells knocked down with FKBP1A (Fig. 2C). The concentration of ALT and AST released from the cells was detected by ELISA (Fig. 2D). LPS increased the release of injury factors, which was ameliorated in AP-treated cells, and the knockdown of FKBP1A blocked the AP effect. Using the TUNEL assay, it was observed that AP ameliorated LPS-induced apoptosis, which was dependent on FKBP1A expression (Fig. 2E).

Knockdown of FKBP1A activates NOTCH1 and reverses the effect of AP on mice with ALI

The lentivirus of sh-FKBP1A #1 (named LV-FKBP1A^{KD}) was administrated via the tail vein and combined with AP (100 mg/kg) treatment and

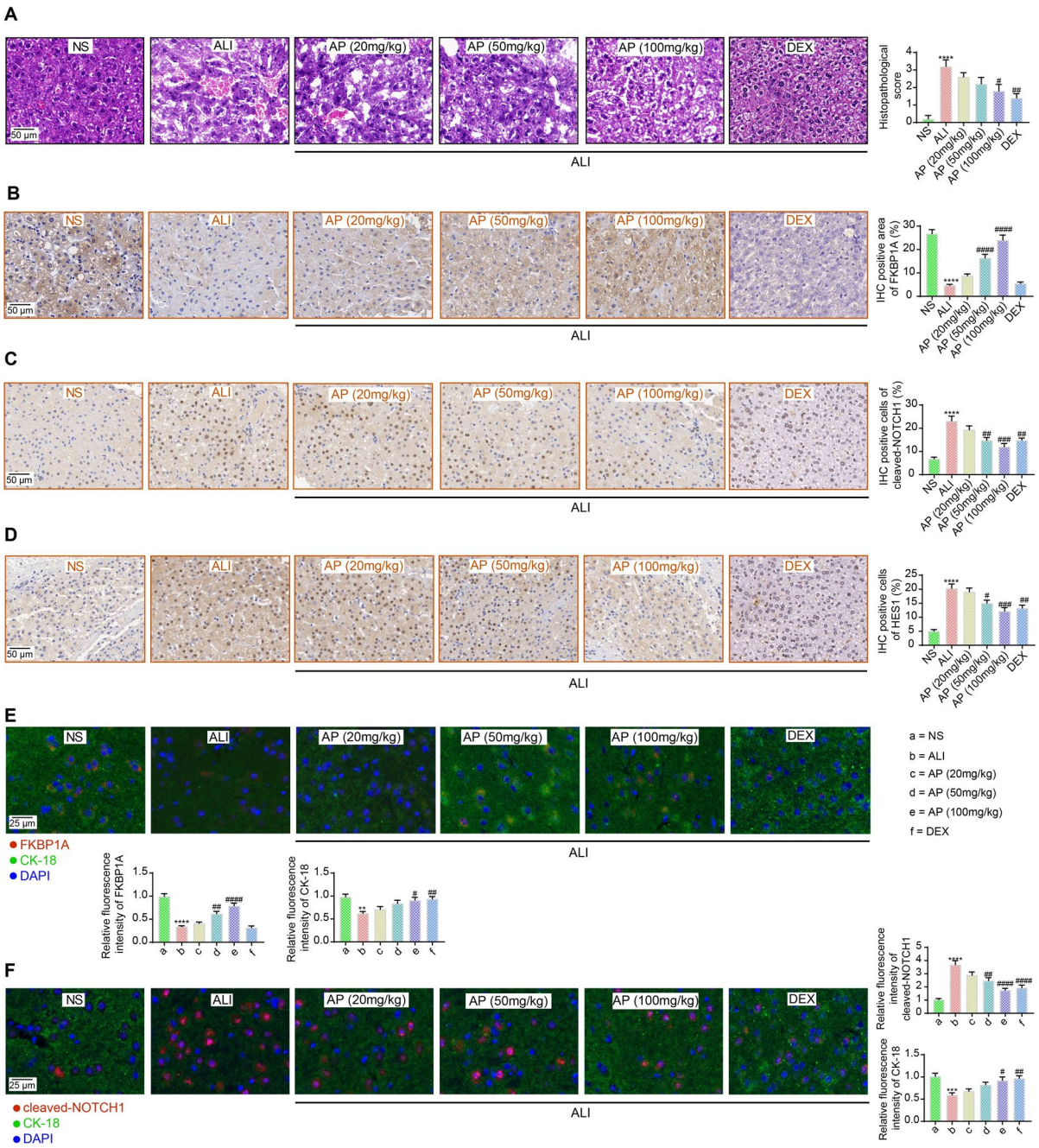

Fig. 1 AP affects FKBP1A/NOTCH1 signaling in the liver parenchymal cells of ALI mice. (**A**) Modeling of ALI and AP or DEX treatment detected by HE staining ($n=5$). IHC detection of FKBP1A (**B**), cleaved NOTCH1 (**C**), and HES1 (**D**) in mouse liver tissues ($n=5$). Changes in FKBP1A (**E**) and cleaved-NOTCH1 (**F**) expression in liver parenchymal cells (CK-18-positive) analyzed by dual-labeling IHC. Data are mean ± SEM, $^{****}p<0.0001$, $\#p<0.05$, $\#\#p<0.01$, $\#\#\#p<0.001$, $\#\#\#\#p<0.0001$ by one-way ANOVA followed by Tukey's (**B**-**F**) test

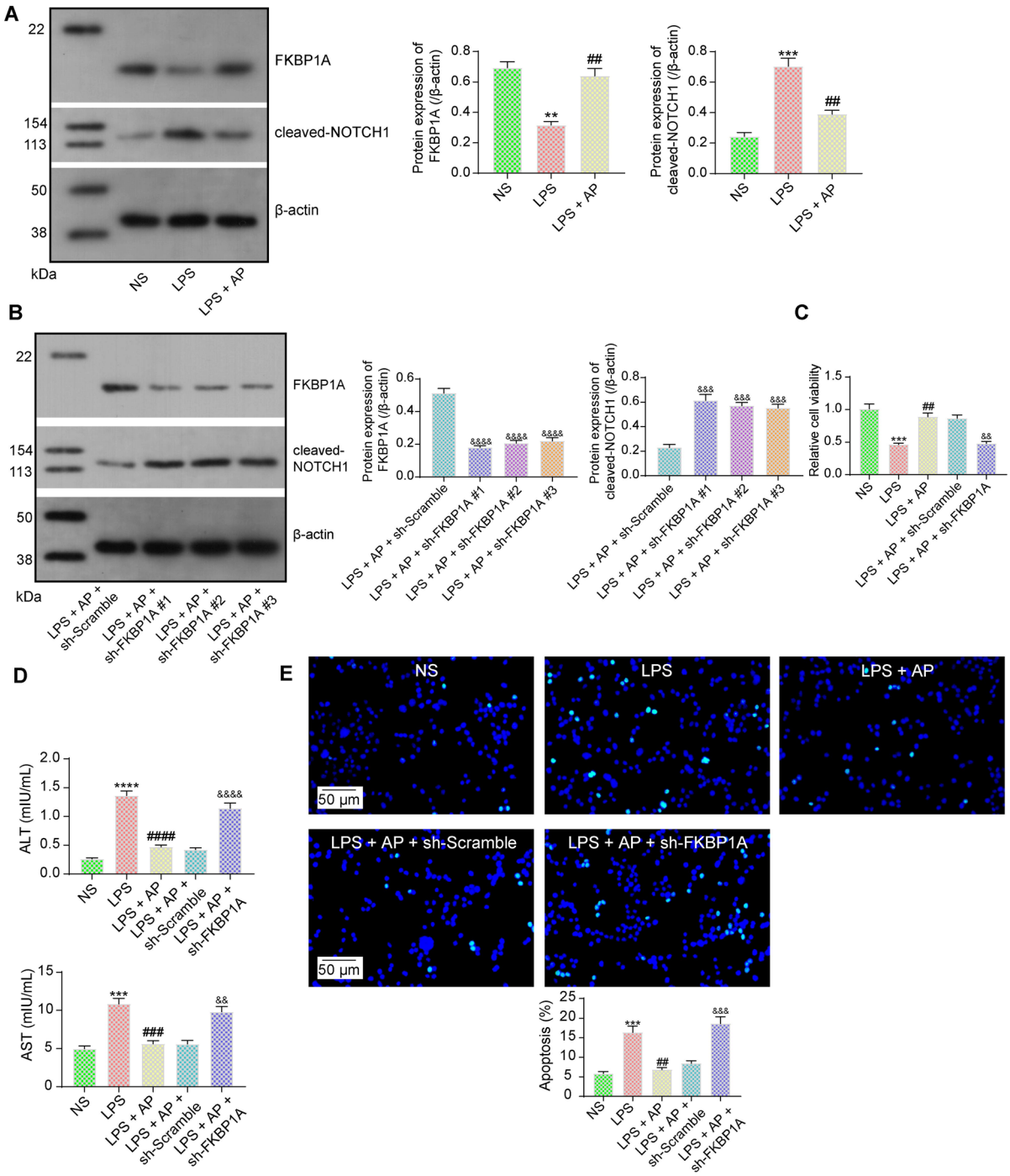

ALI modeling (Fig. S3A). LV-FKBP1A^{KD} injection resulted in reduced survival in mice (Fig. S3B).

LV-FKBP1A^{KD} successfully inhibited the protein expression of FKBP1A in liver tissues and promoted the expression of active NOTCH1 and HES1 as detected by IHC (Fig. 3A). Knockdown of FKBP1A increased hepatocyte necrosis and histopathological scores, as revealed by HE staining (Fig. 3B). ELISA detected that the knockdown of FKBP1A increased the concentrations of liver injury markers ALT, AST,

◂**Fig. 2** AP attenuates LPS-induced liver parenchymal cell injury in an FKBP1A-dependent manner. (**A**) The effect of LPS and AP treatment on the protein expression of FKBP1A and cleaved NOTCH1 in liver parenchymal cells was examined using western blot assays. (**B**) The effect of shRNAs targeting FKBP1A on the protein expression of FKBP1A and cleaved NOTCH1 was examined using western blot assays. (**C**) Effects of LPS and AP treatment and combined knockdown of FKBP1A on liver parenchymal cell viability were assessed using CCK-8. (**D**) Effect of LPS and AP treatment and combined knockdown of FKBP1A on ALT and AST release from liver parenchymal cells detected by ELISA. (**E**) Effect of LPS and AP treatment and combined knockdown of FKBP1A on apoptosis in liver parenchymal cells detected by TUNEL. Data are mean ± SEM ($n = 3$), $^{**}p < 0.01$, $^{***}p < 0.001$, $^{****}p < 0.0001$, $^{\#\#}p < 0.01$, $^{\#\#\#}p < 0.001$, $^{\#\#\#\#}p < 0.0001$, $^{\&\&}p < 0.01$, $^{\&\&\&}p < 0.001$, $^{\&\&\&\&}p < 0.0001$ by one-way ANOVA followed by Dunnett's (**B**) or Tukey's test (**A**, **C**, **D**, **E**)

and inflammatory cytokines IFN-γ, and TNF-α in the serum of animals (Fig. 3C).

NOTCH1 mediates AK2 transcription in liver parenchymal cells

The downstream mechanisms by which NOTCH1 acts as a transcription factor to promote ALI progression have not been investigated. We downloaded the top 50 target genes of NOTCH1 in hTFtarget (http://bioinfo.life.hust.edu.cn/hTFtarget/#!/) and had them cross-screened with the differentially expressed genes in the GSE166868 dataset, and there were two intersecting targets: LASP1 and AK2 (Fig. S4A). ChIP-seq samples of mouse NOTCH1 were selected in the Cistrome Data Browser (http://cistrome.org/db/#/) to predict NOTCH1 binding at the promoter regions of LASP1 and AK2 (Fig. S4B). We observed a specific enrichment of NOTCH1 around the AK2, but not the LASP1 promoter, suggesting that NOTCH1 may specifically regulate the transcription of AK2.

The overexpression plasmid of NOTCH1 was transfected in liver parenchymal cells, and NOTCH1 overexpression promoted the expression of AK2 but had an insignificant effect on the LASP1 expression (Fig. 4A). The effects of LPS, AP treatment, and intervention of FKBP1A on AK2 expression in liver parenchymal cells were examined by RT-qPCR (Fig. 4B). LPS treatment induced AK2 expression in liver parenchymal cells, which was inhibited AP treatment, and knockdown of FKBP1A rescued AK2 expression. ChIP-qPCR assays confirmed the binding ability of NOTCH1 to the AK2 promoter (Fig. 4C), while overexpression of NOTCH1 significantly enhanced the promoter transcriptional activity of AK2 (Fig. 4D).

AP-mediated FKBP1A expression alleviates ALI-induced ER stress

The expression of CHOP and GRP78 was elevated in liver tissues of ALI mice as detected by IHC, and the ER stress was inhibited by AP treatment in liver tissues and reversed by knockdown of FKBP1A (Fig. 5A, B). Meanwhile, significantly enhanced expression of CHOP and GRP78 in LPS-treated liver parenchymal cells was observed using western blot assays, and AP treatment inhibited the ER stress pathway in an FKBP1A-dependent manner (Fig. 5C).

The ameliorating effect of AP on LPS-induced ER stress in the liver parenchymal cells was significantly reversed by overexpression of NOTCH1. In contrast, the NOTCH1-activated ER stress pathway was significantly blocked by knocking down AK2 expression using shRNAs (Fig. 5D). sh-AK2 #1, which had the best knockdown effect, was chosen for subsequent experiments.

NOTCH1-mediated AK2 reverses the protective effect of AP on liver parenchymal cells

CCK8 assay detected that NOTCH1 expression was detrimental to the cytoprotective effects of AP, whereas cell viability was rescued by knocking down AK2 (Fig. 6A). TUNEL assays observed that NOTCH1 expression led to enhanced apoptosis in liver parenchymal cells, while knockdown of AK2 expression inhibited apoptosis in liver parenchymal cells (Fig. 6B). The overexpression of NOTCH1 increased the levels of ALT and AST released by the cells as detected by ELISA. Again, knockdown of AK2 expression ameliorated the liver parenchymal cell injury (Fig. 6C, D).

Activation of NTOCH1 accentuates ALI in mice via the ER stress pathway

A lentivirus overexpressing NOTCH1 (LV-NOTCH1^{OE}) was injected into mice, and an ER stress inhibitor TUDCA was administrated into mice while receiving AP treatment (Fig. S5A).

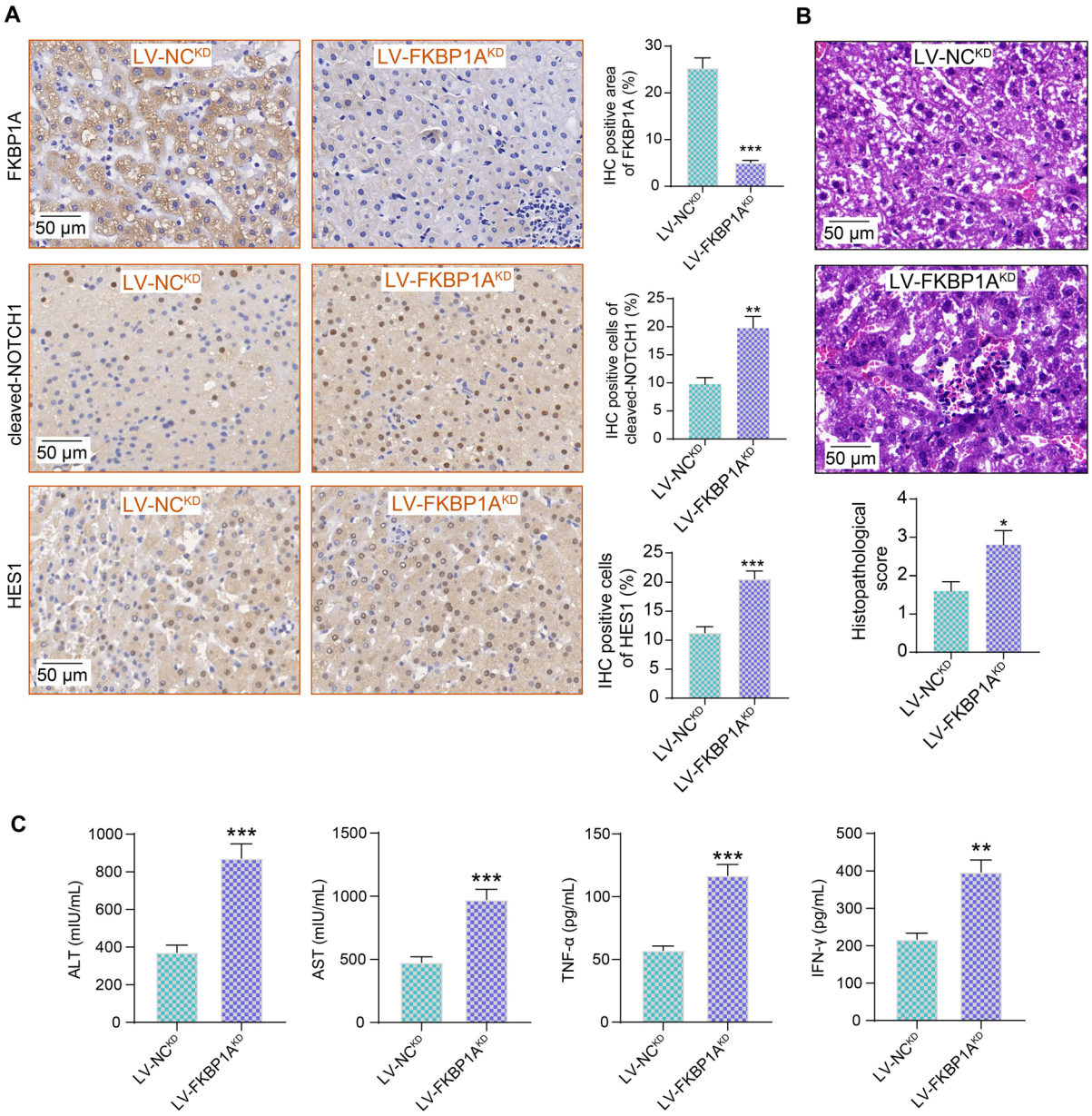

Fig. 3 FKBP1A expression is involved in the protective effect of AP against ALI. (**A**) The effect of LV-FKBP1A^{KD} injection on the expression of FKBP1A, cleaved-NOTCH1, and HES1 in mouse liver tissues was examined using IHC staining ($n=5$). (**B**) Structural changes in liver pathology caused by knockdown of FKBP1A detected by HE staining ($n=5$). (**C**) Serum cytokine concentrations in mice with ALI caused by knockdown of FKBP1A were analyzed using ELISA ($n=5$). Data are mean ± SEM, $^{*}p<0.05$, $^{**}p<0.01$, $^{***}p<0.001$ by unpaired t-test

LV-NOTCH1^{OE}-treated mice showed death within 36 h after ALI modeling, whereas no death of animals occurred in the remaining two groups within 36 h (Fig. S5B).

The protein expression of cleaved-NOTCH1 (Fig. 7A), HES1 (Fig. 7B), AK2 (Fig. 7C), CHOP (Fig. 7D), and GRP78 (Fig. 7E) in liver tissues was examined using IHC assays. LV-NOTCH1^{OE}

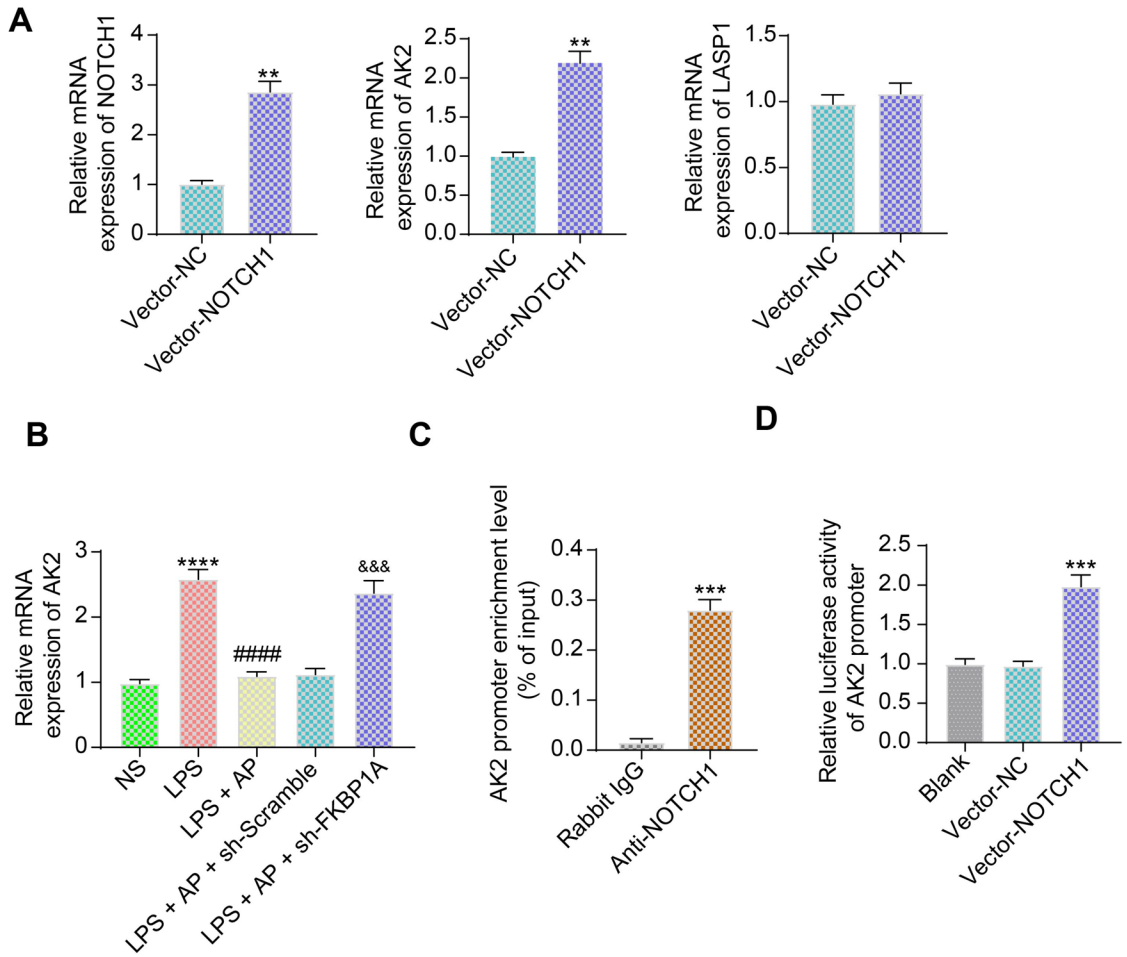

Fig. 4 NOTCH1 mediates AK2 transcription in liver parenchymal cells. (**A**) Effect of overexpression of NOTCH1 on the expression of AK2 and LASP1 in liver parenchymal cells detected by RT-qPCR. (**B**) Effect of LPS, AP treatment, and combined knockdown of FKBP1A on AK2 expression in liver parenchymal cells detected by RT-qPCR. (**C**) Detection of NOTCH1 binding ability to the AK2 promoter was analyzed using ChIP-qPCR. (**D**) The effect of NOTCH1 on the transcriptional activity of the AK2 promoter was analyzed using a dual-luciferase reporter assay. Data are mean ± SEM ($n = 3$), $^{**}p < 0.01$, $^{***}p < 0.001$, $^{****}p < 0.0001$, $\#\#\#\#p < 0.0001$, $\&\&\&p < 0.001$ by unpaired t-test (**A**, **C**) or one-way ANOVA followed by Tukey's (**B**, **D**) test

significantly increased NOTCH1 expression in mouse liver tissues, thereby upregulating HES1, AK2, CHOP, and GRP78 protein expression. In contrast, TUDCA treatment suppressed ER stress in the liver, while having no impact on the expression of NOTCH1 and AK2. HE staining visualized NOTCH1-induced liver parenchymal cell injury, and blocking NOTCH1-activated ER stress significantly improved ALI (Fig. 7F). NOTCH1 upregulation led to an increase in apoptotic cells in liver tissues, which was significantly reduced after blocking the ER pathway using TUDCA (Fig. 7G).

Discussion

AP has been recently highlighted to affect various cellular processes, including ER stress, lipid droplet accumulation, reactive oxygen species levels, and compromised cell integrity, while the understanding of the underlying mechanisms remains limited (Banerjee et al. 2020; Phetruen et al. 2023). Here, AP was revealed to have a protective effect against D-galactosamine and LPS-induced ALI, promote the survival of mice, and relieve ER stress by blocking NOTCH1-mediated AK2 via FKBP1A.

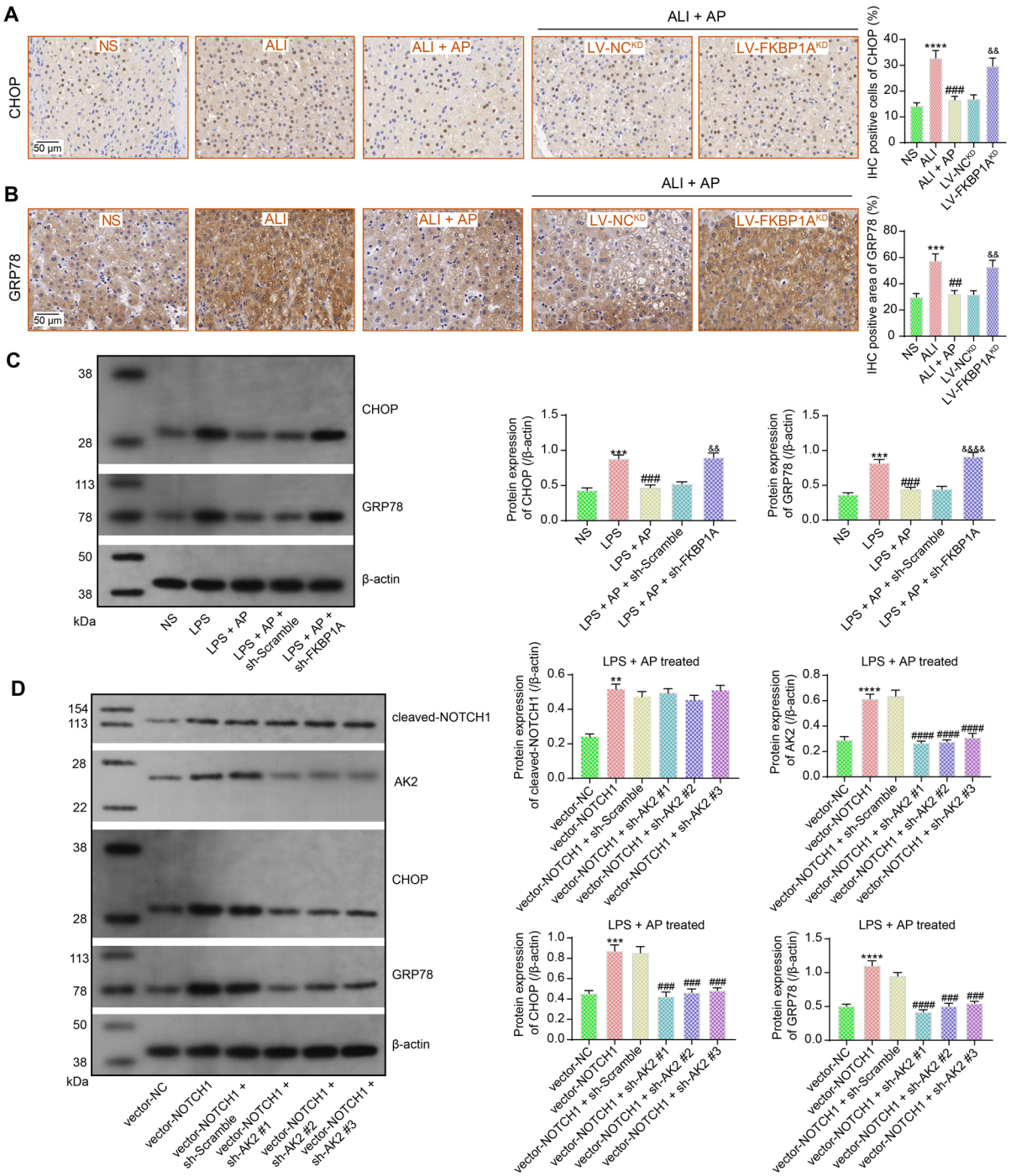

Fig. 5 NOTCH1/AK2 is an effector pathway for AP blockade of ER stress. Expression of ER stress marker proteins CHOP (**A**) and GRP78 (**B**) in liver tissues of the mice treated with AP and FKBP1A knockdown detected by IHC ($n=5$). (**C**) Effects of LPS and AP treatment and combined knockdown of FKBP1A on CHOP and GRP78 expression in liver parenchymal cells ($n=3$). (**D**) Vector-NOTCH1 and sh-AK2 on NOTCH1, AK2, CHOP and GRP78 expression in liver parenchymal cells ($n=3$). Data are mean ± SEM, $^{**}p<0.01$, $^{***}p<0.001$, $^{****}p<0.0001$, $\#\#p<0.01$, $\#\#\#p<0.001$, $\#\#\#\#p<0.0001$, $\&\&p<0.01$, $\&\&\&\&p<0.0001$ by one-way ANOVA followed by Tukey's (A-D) test

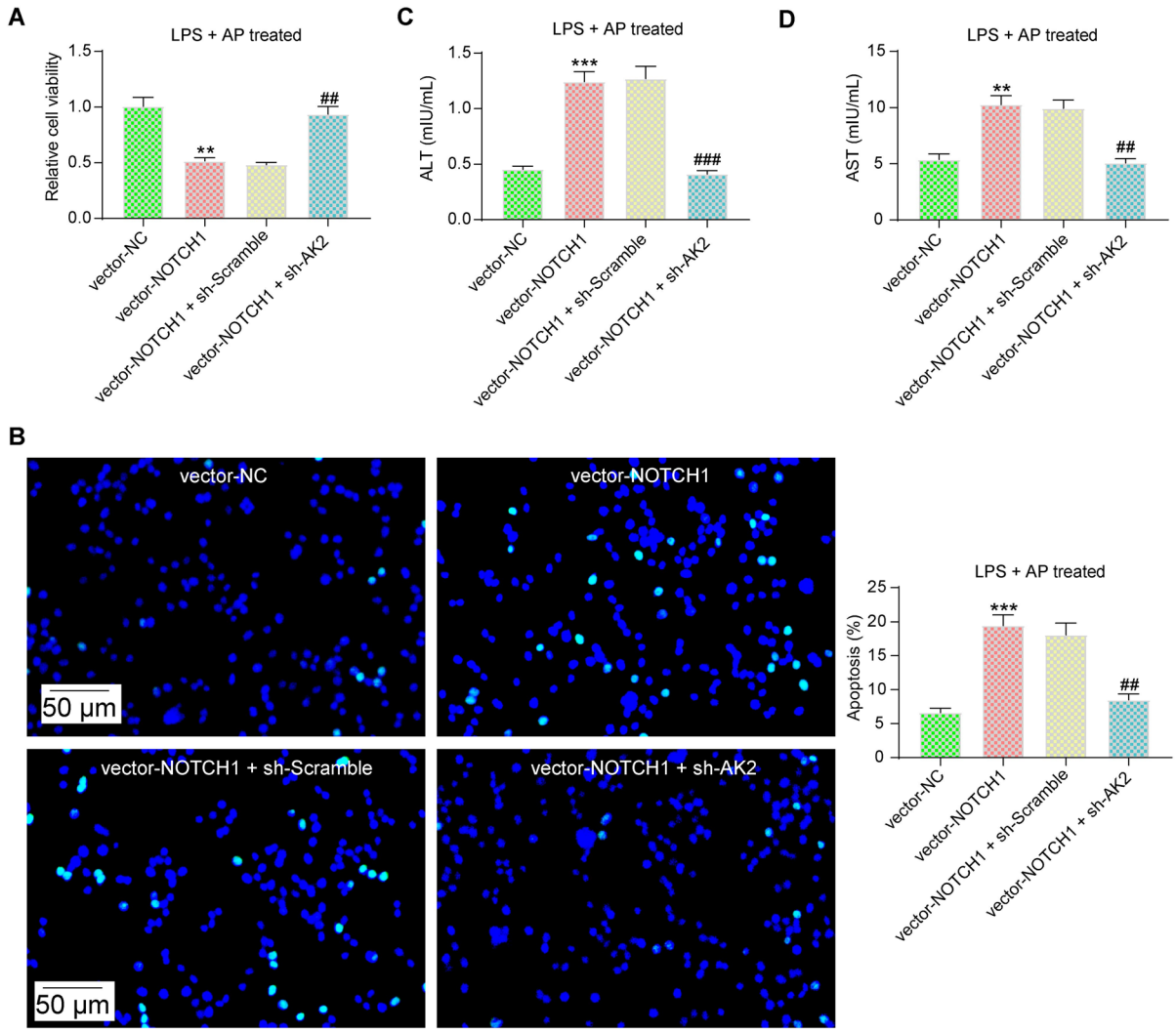

Fig. 6 AP impairs the NOTCH1/AK2 pathway to ameliorate LPS-induced liver parenchymal cell injury. (**A**) Effects of NOTCH1/AK2 alteration on liver parenchymal cell viability were assessed using CCK-8. (**B**) Effect of NOTCH1/AK2 alteration on apoptosis in liver parenchymal cells detected by TUNEL. (**C-D**) Effect of NOTCH1/AK2 alteration on ALT and AST release from liver parenchymal cells detected by ELISA. Data are mean ± SEM ($n = 3$), $^{**}p < 0.01$, $^{***}p < 0.001$, $^{\#\#}p < 0.01$, $^{\#\#\#}p < 0.001$ by one-way ANOVA followed by Tukey's test

A recent study has demonstrated that AP sodium bisulfite significantly alleviates the clinical symptoms of ulcerative colitis and liver injury by reducing the disease activity index (Guan et al. 2022). In addition, Andro-III, derived from the structural modification of AP, possessed anti-inflammatory and neuroprotective effects in vitro and in 3xTg-AD mice (Hu et al. 2024). More relevantly, AP derivative protected acute liver damage in mice by blocking STAT3 activation (Chen et al. 2018). However, these two reports only validated the regulatory effects of AP on the downstream signaling pathways, the physical targets of AP have not been dissected. Here, we identified FKBP1A and its target NOTCH1 as the molecules controlled by AP and found the dose-dependent modulation of FKBP1A and NOTCH1 in the liver tissues of mice pre-treated with AP and induced with ALI. More importantly, we found that there were no cytotoxic effects of AP on liver parenchymal cells until 60 μM. Knockdown of FKBP1A using two shRNAs, by

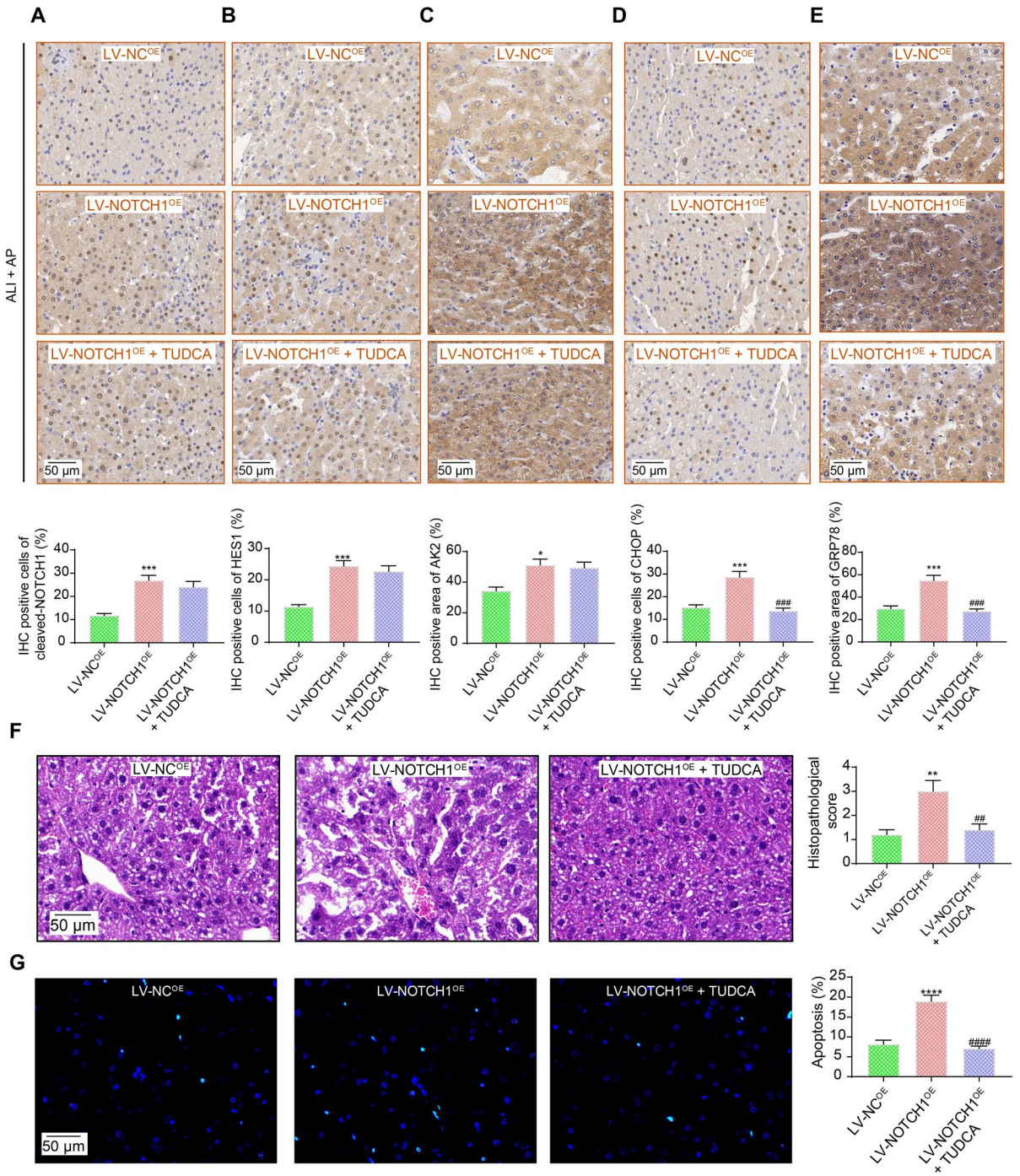

Fig. 7 AP-mediated signaling ameliorates ALI by blocking ER stress. The effect of LV-NOTCH1^{OE} injection and TUDCA on the expression of NOTCH1 (**A**), HES1 (**B**), AK2 (**C**), CHOP (**D**), and GRP78 (**E**) in mouse liver tissues was examined using IHC staining ($n=5$). (**F**) Structural changes in liver pathology caused by LV-NOTCH1^{OE} injection and TUDCA detected by HE staining ($n=5$). (**G**) Effect of overexpression of NOTCH1 and blockade of ER stress pathway on apoptosis in the liver of mice detected by TUNEL ($n=5$). Data are mean ± SEM, $^{*}p<0.05$, $^{**}p<0.01$, $^{***}p<0.001$, $^{****}p<0.0001$, $^{\#\#}p<0.01$, $^{\#\#\#}p<0.001$, $^{\#\#\#\#}p<0.0001$ by one-way ANOVA followed by Tukey's test

contrast, ablated the protective effects of AP on liver parenchymal cells.

FKBP1A-encoded FKBP12, a 12-kDa globular cytosolic protein, is the archetypal member of the immunophilin family (Caminati and Procacci 2020). As we mentioned above, AP can elicit anti-inflammatory effects through different pathways and targets, including regulation of the secretion of inflammatory mediators (Cai et al. 2022). In this study, the suppressing effects of AP on AST and ALT were neutralized following the knockdown of FKBP1A using shRNA lentivirus. Dendrobine has also been reported to reduce the levels of proinflammatory factors, oxidative stress levels, and apoptosis levels in human umbilical vein endothelial cells induced by oxidized low-density lipoprotein via the promotion of FKBP1A (Lou et al. 2022). As for its sole role, FKBP1A acted as a target protein in mediating necroptosis and the related systemic inflammatory response syndrome triggered by TNF-α (Wang et al. 2019). These reports partially substantiated the role of FKBP1A during the inflammatory response. However, its relation to the ALI has not been revealed yet. Our in vitro and in vivo findings linked the hepatoprotective effects of AP to FKBP1A-controlled NOTCH1 activation, which underscores the novelty of this study. The Notch intracellular domain is cleaved and translocates to the nucleus, thus forming a transactivation complex, and the primary Notch target genes include two families of transcriptional factors, namely Hes, which includes HES1 and HES5, and Hairy/Enhancer-of-split-related with YRPW motif (Gallenstein et al. 2023). The intracellular domain of NOTCH1 has been widely implicated in multiple cell injury caused by LPS-induced sepsis and related complications (Li et al. 2023; Liu et al. 2023; Wang et al. 2023; Xu et al. 2024).

Subsequently, AK2 was identified to be the target of NOTCH1 in ALI since NOTCH1 overexpression did not lead to LASP1 expression alteration. AK2 is found in the mitochondrial intermembrane region and is expressed at high levels in the liver, kidneys, and heart (Fujisawa 2023). ER of all eukaryotic cells is a membrane-bound organelle, and the accumulation of drugs/chemicals/xenobiotics in the cytosol can trigger ER stress which is recognized by the accumulation of unfolded or misfolded proteins in the lumen of ER (Rana 2020). Considering the importance of AK2 to ER stress (Burkart et al. 2011) and the contribution of ER stress to ALI and sepsis-related complications (Chen et al. 2024; Park et al. 2023; Wang et al. 2024; Wu et al. 2016), we assessed the ER stress marker proteins in the liver tissues of mice and liver parenchymal cells, respectively. Here, the suppressing

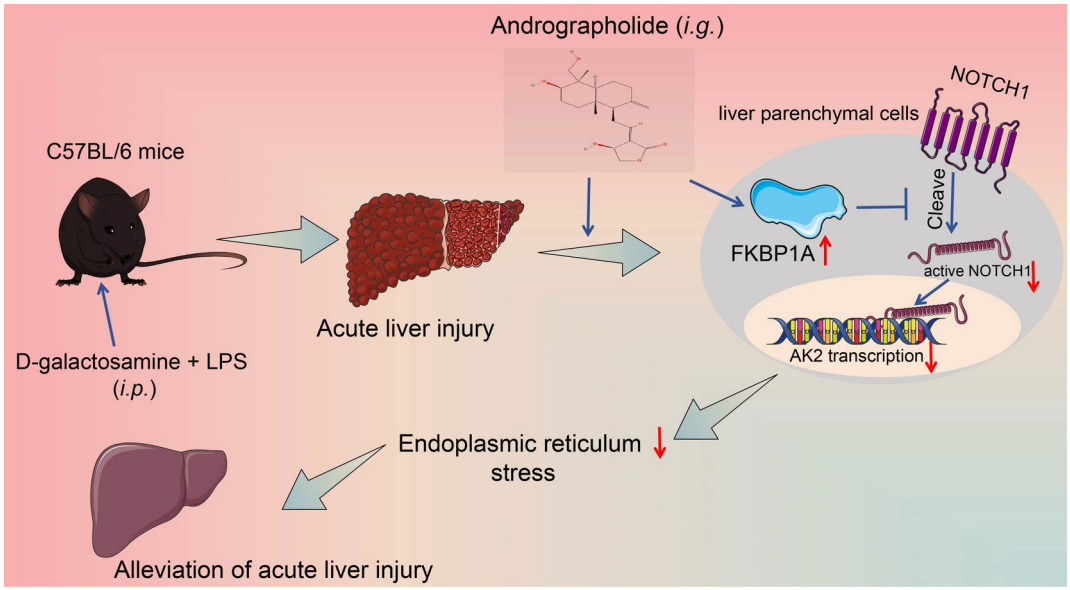

Fig. 8 Model of AP mechanism of action in alleviating ALI. AP-mediated FKBP1A expression inhibits ALI progression by inhibiting NOTCH1-mediated AK2 transcription and blocking the ER stress pathway

effects of AP on the protein expression of CHOP and GRP78 were reversed by FKBP1A knockdown or NOTCH1 overexpression. Knockdown of AK2, similarly exerted the halting effects on ER stress in the presence of NOTCH1 overexpression in vitro. Lee et al. showed that hepatocytes treated with TUDCA showed suppression of ER stress, and reduced inflammation and cell death (Lee et al. 2020). We further validated these results in vivo in mice treated with NOTCH1 overexpression and found that survival was prolonged and the injury was alleviated in these animals, suggesting that ER stress is indeed the effector mechanism that contributes to AP-mediated ALI alleviation.

Our study has some limitations. Firstly, we do not provide transmission electron microscopy to examine the ultrastructure of liver parenchymal cells. This limits us to observing ER morphology within cells. In addition, the small number of animals assessed for survival ($n=8$) resulted in the observation of some groups with 100% survival. Further studies should consider incorporating more mice to enhance the reliability of our research.

Conclusion

In conclusion, we demonstrated that AP-induced FKBP1A represses NOTCH1 activation, which in turn inhibits AK2 transcription and the ER stress pathway in ALI (Fig. 8). By identifying the molecular pathways through which AP-mediated FKBP1A/NOTCH1/AK2 signaling regulates ER stress, our findings provide a rationale for the refinement of therapeutic approaches to alleviate ALI for patients in the ICU.

Acknowledgements We thank to Key Research and Development Project of Hainan Province (No. ZDYF2022SHFZ118) and Hainan Province 'Nanhai Xinxing' Medical and Health Talent Platform Project for the funding support.

Author contributions JQH conceived and designed the experiments and produced the initial draft of the manuscript. ZPH collected the data and carried out the data analyses and statistical analysis. RZ provided resources, supervision, and review of the manuscript. All the authors have read and approved the final submitted manuscript.

Funding This study was supported by the Key Research and Development Project of Hainan Province (No. ZDYF2022SHFZ118) and Hainan Province's Nanhai Xinxing' Medical and Health Talent Platform Project.

Data availability The data that support the findings of this study are available from the corresponding author upon reasonable request.

Declarations

Ethical approval The study protocols were approved by the Institutional Animal Care and Use Committee of the Huadong Hospital Affiliated to Fudan University. The animals received humane care according to the criteria outlined in the Guide for the Care and Use of Laboratory Animals published by the NIH.

Consent for publication Not applicable.

Conflict of interests The authors declare no competing interests.

References

Banerjee A, Czinn SJ, Reiter RJ, Blanchard TG. Crosstalk between endoplasmic reticulum stress and anti-viral activities: A novel therapeutic target for COVID-19. Life Sci. 2020;255:117842. https://doi.org/10.1016/j.lfs.2020.117842.

Burkart A, Shi X, Chouinard M, Corvera S. Adenylate kinase 2 links mitochondrial energy metabolism to the induction of the unfolded protein response. J Biol Chem. 2011;286(6):4081–9. https://doi.org/10.1074/jbc.M110.134106.

Bustin SA, Benes V, Garson JA, et al. The MIQE guidelines: minimum information for publication of quantitative real-time PCR experiments. Clin Chem. 2009;55(4):611–22. https://doi.org/10.1373/clinchem.2008.112797.

Cai Q, Zhang W, Sun Y, Xu L, Wang M, Wang X, et al. Study on the mechanism of andrographolide activation. Front Neurosci. 2022;16:977376. https://doi.org/10.3389/fnins.2022.977376.

Caminati G, Procacci P. Mounting evidence of FKBP12 implication in neurodegeneration. Neural Regen Res. 2020;15(12):2195–202. https://doi.org/10.4103/1673-5374.284980.

Cecconi M, Evans L, Levy M, Rhodes A. Sepsis and septic shock. Lancet. 2018;392(10141):75–87. https://doi.org/10.1016/S0140-6736(18)30696-2.

Chen H, Zhang W, Sun X, et al. Fkbp1a controls ventricular myocardium trabeculation and compaction by regulating endocardial Notch1 activity. Development. 2013;140(9):1946–57. https://doi.org/10.1242/dev.089920.

Chen SR, Li F, Ding MY, et al. Andrographolide derivative as STAT3 inhibitor that protects acute liver damage in mice. Bioorg Med Chem. 2018;26(18):5053–61. https://doi.org/10.1016/j.bmc.2018.09.002.

Chen Y, Zhao J, Ye H, et al. Beneficial impact of cardiac heavy metal scavenger metallothionein in sepsis-provoked cardiac anomalies dependent upon regulation of endoplasmic reticulum stress and ferroptosis but not autophagy. Life Sci. 2024;336:122291. https://doi.org/10.1016/j.lfs.2023.122291.

Dai Y, Chen SR, Chai L, Zhao J, Wang Y, Wang Y. Overview of pharmacological activities of Andrographis paniculata and its major compound andrographolide. Crit Rev Food Sci Nutr. 2019;59(sup1):S17–29. https://doi.org/10.1080/10408398.2018.1501657.

de Perez Ruiz Garibay A, Kortgen A, Leonhardt J, Zipprich A, Bauer M. Critical care hepatology: definitions, incidence, prognosis and role of liver failure in critically ill patients. Crit Care. 2022;26(1):289. https://doi.org/10.1186/s13054-022-04163-1.

Du Z, Wei C, Yan J, et al. Mesenchymal stem cells overexpressing C-X-C chemokine receptor type 4 improve early liver regeneration of small-for-size liver grafts. Liver Transpl. 2013;19(2):215–25. https://doi.org/10.1002/lt.23577.

Fujisawa K. Regulation of adenine nucleotide metabolism by adenylate kinase isozymes: physiological roles and diseases. Int J Mol Sci. 2023;24(6):5561. https://doi.org/10.3390/ijms24065561.

Gallenstein N, Tichy L, Weigand MA, Schenz J. Notch signaling in acute inflammation and sepsis. Int J Mol Sci. 2023;24(4):3458. https://doi.org/10.3390/ijms24043458.

Gant JC, Blalock EM, Chen KC, et al. FK506-binding protein 1b/12.6: a key to aging-related hippocampal Ca2+ dysregulation? Eur J Pharmacol. 2014;739:74–82. https://doi.org/10.1016/j.ejphar.2013.10.070.

Guan F, Luo H, Wu J, et al. Andrographolide sodium bisulfite ameliorates dextran sulfate sodium-induced colitis and liver injury in mice via inhibiting macrophage proinflammatory polarization from the gut-liver axis. Int Immunopharmacol. 2022;110:109007. https://doi.org/10.1016/j.intimp.2022.109007.

Hu M, Zheng M, Wang C, Li Q, Li J, Zhou X, et al. Andrographolide derivative Andro-III modulates neuroinflammation and attenuates neuropathological changes of Alzheimer's disease via GSK-3beta/NF-kappaB/CREB pathway. Eur J Pharmacol. 2024;965:176305. https://doi.org/10.1016/j.ejphar.2023.176305.

Lee CH, Han JH, Kim S, et al. Metformin ameliorates bile duct ligation-induced acute hepatic injury via regulation of ER stress. BMB Rep. 2020;53(6):311–6. https://doi.org/10.5483/BMBRep.2020.53.6.169.

Li G, Hu C, Liu Y, Lin H. Ligustilide, a novel SIRT1 agonist, alleviates lipopolysaccharide-induced acute lung injury through deacetylation of NICD. Int Immunopharmacol. 2023;121:110486. https://doi.org/10.1016/j.intimp.2023.110486.

Li Y, Huang L, Li J, et al. Targeting TLR4 and regulating the Keap1/Nrf2 pathway with andrographolide to suppress inflammation and ferroptosis in LPS-induced acute lung injury. Chin J Nat Med. 2024;22(10):914–28. https://doi.org/10.1016/S1875-5364(24)60727-2.

Liu J, Du S, Kong Q, et al. HSPA12A attenuates lipopolysaccharide-induced liver injury through inhibiting caspase-11-mediated hepatocyte pyroptosis via PGC-1alpha-dependent acyloxyacyl hydrolase expression. Cell Death Differ. 2020;27(9):2651–67. https://doi.org/10.1038/s41418-020-0536-x.

Liu T, Zhang C, Ying J, et al. Inhibition of the intracellular domain of Notch1 results in vascular endothelial cell dysfunction in sepsis. Front Immunol. 2023;14:1134556. https://doi.org/10.3389/fimmu.2023.1134556.

Lou D, Xing X, Liang Y. Dendrobine modulates autophagy to alleviate ox-LDL-induced oxidative stress and senescence in HUVECs. Drug Dev Res. 2022;83(5):1125–37. https://doi.org/10.1002/ddr.21937.

Low M, Suresh H, Zhou X, et al. The wide spectrum anti-inflammatory activity of andrographolide in comparison to NSAIDs: A promising therapeutic compound against the cytokine storm. PLoS One. 2024;19(7):e0299965. https://doi.org/10.1371/journal.pone.0299965.

Nesseler N, Launey Y, Aninat C, et al. Clinical review: The liver in sepsis. Crit Care. 2012;16(5):235. https://doi.org/10.1186/cc11381.

Nesseler N, Launey Y, Aninat C, et al. Liver dysfunction is associated with long-term mortality in septic shock. Am J Respir Crit Care Med. 2016;193(3):335–7. https://doi.org/10.1164/rccm.201508-1660LE.

Park SH, Seo W, Xu MJ, et al. Ethanol and its Nonoxidative Metabolites Promote Acute Liver Injury by Inducing ER Stress, Adipocyte Death, and Lipolysis. Cell Mol Gastroenterol Hepatol. 2023;15(2):281–306. https://doi.org/10.1016/j.jcmgh.2022.10.002.

Phetruen T, van Dam B, Chanarat S. Andrographolide induces ROS-mediated cytotoxicity, lipid peroxidation, and compromised cell integrity in saccharomyces cerevisiae. Antioxidants (Basel). 2023;12(9):1765. https://doi.org/10.3390/antiox12091765.

Qin Y, Wang Y, Liu O, et al. tauroursodeoxycholic acid attenuates angiotensin II induced abdominal aortic aneurysm formation in apolipoprotein E-deficient mice by inhibiting endoplasmic reticulum stress. Eur J Vasc Endovasc Surg. 2017;53(3):337–45. https://doi.org/10.1016/j.ejvs.2016.10.026.

Qin X, Wang X, Tian M, et al. The role of Andrographolide in the prevention and treatment of liver diseases.

Phytomedicine. 2023;109:154537. https://doi.org/10.1016/j.phymed.2022.154537.
Rana SVS. Endoplasmic reticulum stress induced by toxic elements-a review of recent developments. Biol Trace Elem Res. 2020;196(1):10–9. https://doi.org/10.1007/s12011-019-01903-3.
Rudd KE, Johnson SC, Agesa KM, et al. Global, regional, and national sepsis incidence and mortality, 1990–2017: analysis for the global burden of disease study. Lancet. 2020;395(10219):200–11. https://doi.org/10.1016/S0140-6736(19)32989-7.
Santos FA, Silva RM, Tome AR, et al. 1,8-cineole protects against liver failure in an in-vivo murine model of endotoxemic shock. J Pharm Pharmacol. 2001;53(4):505–11. https://doi.org/10.1211/0022357011775604.
Shu L, Fu H, Pi A, et al. Protective effect of andrographolide against ulcerative colitis by activating Nrf2/HO-1 mediated antioxidant response. Front Pharmacol. 2024;15:1424219. https://doi.org/10.3389/fphar.2024.1424219.
Strnad P, Tacke F, Koch A, Trautwein C. Liver - guardian, modifier and target of sepsis. Nat Rev Gastroenterol Hepatol. 2017;14(1):55–66. https://doi.org/10.1038/nrgastro.2016.168.
Sun J, Zhang J, Wang X, et al. Gut-liver crosstalk in sepsis-induced liver injury. Crit Care. 2020;24(1):614. https://doi.org/10.1186/s13054-020-03327-1.
Tian Q, Liu J, Chen Q, Zhang M. Andrographolide contributes to the attenuation of cardiac hypertrophy by suppressing endoplasmic reticulum stress. Pharm Biol. 2023;61(1):61–8. https://doi.org/10.1080/13880209.2022.2157021.
Tsao PN, Wei SC, Huang MT, et al. Lipopolysaccharide-induced Notch signaling activation through JNK-dependent pathway regulates inflammatory response. J Biomed Sci. 2011;18(1):56. https://doi.org/10.1186/1423-0127-18-56.
Wang Z, Feng J, Yu J, Chen G. FKBP12 mediates necroptosis by initiating RIPK1-RIPK3-MLKL signal transduction in response to TNF receptor 1 ligation. J Cell Sci. 2019;132(10):jcs227777. https://doi.org/10.1242/jcs.227777.
Wang L, Zhao Y, Su Z, Zhao K, Li P, Xu T. Ginkgolide A targets forkhead box O1 to protect against lipopolysaccharide-induced septic cardiomyopathy. Phytother Res. 2023;37(8):3309–22. https://doi.org/10.1002/ptr.7802.
Wang S, Xu F, Liu H, Shen Y, Zhang J, Hu L, et al. Suppressing endoplasmic reticulum stress alleviates lps-induced acute lung injury via inhibiting inflammation and ferroptosis. Inflammation. 2024;47(4):1067–82. https://doi.org/10.1007/s10753-023-01962-8.
Wu FL, Liu WY, Van Poucke S, et al. Targeting endoplasmic reticulum stress in liver disease. Expert Rev Gastroenterol Hepatol. 2016;10(9):1041–52. https://doi.org/10.1080/17474124.2016.1179575.
Wu X, Luo Y, Wang S, et al. AKAP12 ameliorates liver injury via targeting PI3K/AKT/PCSK6 pathway. Redox Biol. 2022;53:102328. https://doi.org/10.1016/j.redox.2022.102328.
Xu Y, Shen B, Pan X, et al. Palmatine ameliorated lipopolysaccharide-induced sepsis-associated encephalopathy mice by regulating the microbiota-gut-brain axis. Phytomedicine. 2024;124:155307. https://doi.org/10.1016/j.phymed.2023.155307.
Yang Y, Ni M, Zong R, et al. Targeting notch1-YAP circuit reprograms macrophage polarization and alleviates acute liver injury in mice. Cell Mol Gastroenterol Hepatol. 2023;15(5):1085–104. https://doi.org/10.1016/j.jcmgh.2023.01.002.
Ye JF, Zhu H, Zhou ZF, et al. Protective mechanism of andrographolide against carbon tetrachloride-induced acute liver injury in mice. Biol Pharm Bull. 2011;34(11):1666–70. https://doi.org/10.1248/bpb.34.1666.
Yu Y, Miao TW, Xiao W, et al. Andrographolide attenuates NLRP3 inflammasome activation and airway inflammation in exacerbation of chronic obstructive pulmonary disease. Drug Des Devel Ther. 2024;18:1755–70. https://doi.org/10.2147/DDDT.S445788.
Zhang Y, Xue W, Zhang W, et al. Histone methyltransferase G9a protects against acute liver injury through GSTP1. Cell Death Differ. 2020;27(4):1243–58. https://doi.org/10.1038/s41418-019-0412-8.
Zhang S, Feng Z, Gao W, et al. Aucubin attenuates liver ischemia-reperfusion injury by inhibiting the HMGB1/TLR-4/NF-kappaB signaling pathway, oxidative stress, and apoptosis. Front Pharmacol. 2020;11:544124. https://doi.org/10.3389/fphar.2020.544124.
Zhou X, Li J, Quan S, et al. Andrographolide improves ApoE4-mediated blood-brain barrier injury by alleviating inflammation. Mol Neurobiol. 2024;61(10):7950–67. https://doi.org/10.1007/s12035-024-04088-6.